The climate change impact on future IDF curves in central Alberta

CCTC 2013 Paper Number 1569716685

C.-C. Kuo [1], N. Jahan [1], M. S. Gizaw [1], T. Y. Gan [1], and S. Chan [2]
[1] University of Alberta, Edmonton, Alberta
[2] City of Edmonton, Edmonton, Alberta

Abstract

A regional climate model, MM5, was set up in a one-way, three-domain nested framework to simulate summer precipitation in central Alberta. MM5 was forced with two sets of GCM (Global Climate Model), CGCM3 and ECHAM5, data for a baseline 1971-2000 and 2041-2100 under SRES (Special Report on Emissions Scenarios) A2. Due to simulation bias, a quantile-based bias correction method was applied to derive grid-based IDF curves. Apparently, projected IDF curves show a higher range of intensities especially for short duration (< 6 hr) storms. More GCMs data should be performed to assess the uncertainties associated with predicting future IDF curves.

Keywords: climate change, MM5, IDF curves

Résumé

Un modèle de climat régional, MM5, a été monté dans un sens unique, dans le cadre niché de trois domaine pour simuler la précipitation d'été dans le centre d'Alberta. Le model MM5 a été forcé avec deux ensembles de GCM (le Modèle de Climat Global), CGCM3 et ECHAM5, les données pour une ligne des bases 1971-2000 et 2041-2100 sous SRES (le Rapport Spécial sur les Scénarios d'Émissions) A2. En raison de l'inclination de simulation, une méthode de correction d'inclination quantile-fondée a été appliquée pour tirer des courbes d'IDF à base de grille. Apparemment, les courbes d'IDF projetées montrent une plus haute gamme d'intensités surtout pour les tempêtes de durée courtes. Plus de données GCMs devraient être exécutées pour évaluer les incertitudes associées à la prédiction des courbes d'IDF futures.

Mots clés : changement climatique, MM5, courbes IDF

1. Introduction

In recent years, central Alberta has experienced numerous severe wet weather events that resulted in considerable damage. While extreme precipitation events such as these are not new, a growing number of studies show that precipitation variability is increasing globally as our planet warms (Dore 2005). Under the impact of global climate change, it is therefore likely that such events will increase in both frequency and in severity. Warmer temperatures have recently been linked to increasing rainfall intensities in many parts of the world (Hamlet and Lettenmaier 2007; Allan and Soden 2008; Lenderink and Meijgaard 2008; Wang et al. 2008), and some streamflow trends indicate increased runoff over the next several decades (Milly et al. 2005). Sun et al. (2007) examined precipitation data from climate change simulations under various IPCC (Intergovernmental Panel on Climate Change) emissions scenarios of the Fourth Assessment (AR4), and concluded that all projections suggested more extreme

precipitation behavior globally, where wet regions may be getting wetter and arid regions may be getting drier. Therefore, the general scientific consensus is that precipitation patterns are changing, but due to the intrinsically high spatial and temporal variability of precipitation, many of the details pertaining to these changes remain uncertain. Through the analysis of observational data, Shen et al. (2005) concluded that over the past century, May – August precipitation has indeed been increasing in Alberta. If storms in this region continue to occur in greater severity, local hydrologic structures will increasingly prove insufficient for handling such rainfall events. The potential evolution of local climate regimes must therefore be taken into consideration when designing future hydrologic structures in central Alberta.

IDF (Intensity-Duration-Frequency) curves, which quantify the expected return period (frequency) of storms with specified intensities and durations, are computed from observed precipitation data. It follows that historic precipitation behavior has traditionally been used to design future hydrologic structures. This type of planning assumes a stationary climate regime, where the future climate is the same as the past climate. However, because global warming could modify the intensity of future extreme precipitation events, structures designed with existing IDF curves may be insufficient. To design adequate municipal structures, which will reduce the negative impacts of extreme rainfall events, future precipitation data are needed.

In recent years, Global Climate Models (GCMs) have been providing insight into how our planet is and will continue to change at the global scale. Because these models are run at relatively coarse spatial resolutions (150-300 km), details pertaining to regional changes particularly in highly variable indices such as precipitation, remain unresolved. High-resolution (1-50 km) RCMs (Regional Climate Models) can thus be used to sort out the details of smaller areas within the global domain, such as the behavior of local precipitation-producing weather systems.

Previous studies have used both GCMs and RCMs to investigate potential global warming-related impacts on precipitation behavior in Canada (Laprise et al. 2003; Mladjic et al. 2011; Mailhot et al. 2012). Some authors have specifically focused on Alberta, such as Shepard and McGinn (2003) who predicted that precipitation will significantly increase in this region, with the largest increases in central Alberta. This is in agreement with Mailhot et al., (2012) who determined that inland regions of Canada (southern Ontario, Prairies, and southern Quebec) will have the largest precipitation increases. While modeling studies tend to agree that precipitation will likely increase in Alberta under global warming, many of them are carried out with spatial resolutions of 45 – 50 km or greater, and generalizations must therefore be made over large areas. To investigate local impacts of climate variability on rainfall behavior, it is necessary to evaluate output from higher-resolution model runs. High-resolution RCM precipitation output can provide the necessary data to generate updated and future IDF curves for regions within Alberta, which will ideally improve and strengthen the safety standards of municipal infrastructures.

2. Research Objectives

The objectives of this paper are (1) to evaluate the climate change impact on IDF curves using MM5 (the Pennsylvania State University / National Center for Atmospheric Research numerical model) and two driven GCMs data under SRES (Special Report on Emissions Scenarios) A2 for Edmonton, (2) to compare the future projected IDF curves and the current used Edmonton IDF curves, and (3) to investigate the air temperature and moisture change and their trends in central Alberta under SRES A2. Section 3 includes the methodology and used data. Section 4 provide the analysed results and the summary and conclusion are in Section 5.

3. Methodology and Data

3.1 MM5 configuration

MM5 was run for May-August for 1971-2000 under 20c3m (twentieth century run) and 2041-2100 under SRES A2. A one-way nesting model configuration was used for three domains, and CGCM3 (The Third Generation Coupled Global Climate Model) and ECHAM5 (the 5th generation of the ECHAM General Circulation Model) data were used as initial and lateral boundary conditions for the most outer domain (D1) with 27-km resolution. The D1 output was then used to run the second 9-km domain (D2), and D2 data were used to run the 3-km innermost domain (D3). The locations of the three domains are illustrated in Figure 1 which contains complex terrains inside the D1 and D2. All these three domains were run with 23 vertical levels.

Erfani et al. (2003) used the Global Environmental Multiscale (GEM) model to examine features of a summertime supercell storm in central Alberta, and found that a 4-km resolution model domain was able to reasonably simulate the system which was initiated along Rocky Mountain foothills. Thus, our spatial resolution should be sufficient to resolve the small-scale convective precipitation events that are common during the summer months, and no cumulus parameterization was used in D2 and D3. High-resolution Blackadar planetary boundary layer (PBL) scheme was used, along with the mixed-phase (Reisner 1; Reisner et al., 1998) explicit moisture scheme, and the rapid and accurate radiative transfer model longwave radiation scheme (RRTM; Mlawer et al., 1997). Because 27-km spatial resolution of D1 is not sufficient to resolve the small-scale convective precipitation events, a cumulus parameterization, Kain-Fritsch 2 (Kain, 2004) cumulus parameterization is applied in the most outer domain (D1).

Deriving IDF curves require sub-hourly precipitation data. Fifteen minute output time step is chosen for D3 to calculate MM5's IDF curves. This output time step is sufficient for IDF curve estimation and yields acceptable file size.

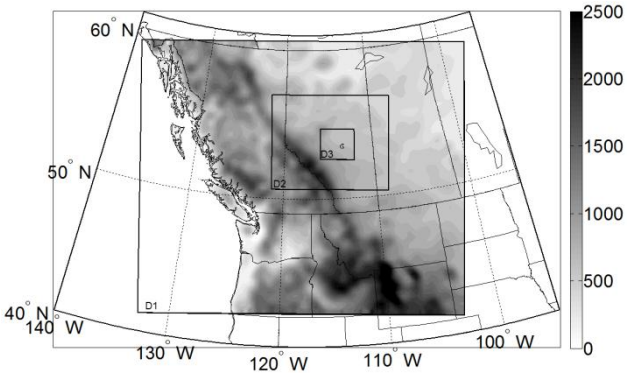

Figure 1. MM5 domain configurations (encompassed by the thin black lines). The outer domain (D1) was run with a 27-km resolution, the second domain was run with a 9-km resolution, and the inner domain (D3) was run with a 3-km resolution.

3.2 Quantiles

In order to compare a large area of IDF curves, we derived IDF curves on the basis of grid cells. The process of obtaining grid based IDF curves is similar to that of single site IDF curves. Each grid is regarded as a single site and the IDF curves are estimated for individual grid in the most inner domain (D3). The probability distribution function used is GEV (General Extreme Value) distribution with parameters derived by the PWM (Probability Weighted Moment), which is confirmed by Kuo et al. (2013) that the GEV-PWM yields more accurate precipitation intensity quantiles than the traditionally fitted probability distribution in Canadian city, the Extreme Value type I (EVI), with parameters derived by the Method of Moment (MOM). Each grid has a set of simulated IDF curves with the duration range from 15-, 30-min, 1-, 2-, 6-, 12- to 24-hr and return periods of 2-, 5-, 10-, 25-, 50-, and 100-yr.

3.3 Bias correction

Evidence of bias in climate model output has made researchers to avoid direct use of climate model precipitation outputs for climate change impact analysis (Lafon et al., 2012; Schmidli et al., 2006; Wood et al, 2004). In our study, significant biases are also noticed in the MM5 simulated precipitation extremes. To correct biases, we used an established bias correction technique called the Quantile Based Bias Correction Method.

The strategy for this quantile based bias removal technique is to match the cumulative distribution function (CDF) of simulated AMP (Annual Maximum Precipitation) to the CDF of observed AMP for individual duration. In this technique, simulated and observed data covering the same period are used to create a ‘quantile map’ of each population using an unbiased quantile estimator applied to the ranked data (Lafon et al., 2012). This quantile map was then used to generate a bias-corrected precipitation time series by replacing the simulated precipitation amount by its value resampled from the distribution fitted to the observations and associated with the same quantile.

Reference IDF curves are obtained either from extreme precipitation data of a single site (at-site analysis) or by combining information from many sites within a region (regional analysis). For sites with sufficient record length as compared to the return period of the extreme quantile of interest, at site frequency analysis can give a reliable estimation. However, sufficient records are not always available. This limitation of records can be overcome by using a regional frequency analysis (RFA; Hosking and Wallis 1997), which trades space for time using observations from different sites (grids) in a given homogeneous region to compensate short or no records at individual sites (grids) within the region. Due to limited rain gauge sites (13 rain gauges) with sufficient record length, reference precipitation extremes at ungauge sites are estimated using regional frequency analysis (RFA) of Hosking and Wallis (1997). RFA provides more robust return period estimates than those estimated using single point data series due to the inclusion of a larger data set (Fowler et al., 2005; Hosking and Wallis, 1997). In this study, individual grid quantiles were obtained from the RFA at the grid box scale (Mailhot et al., 2007) and then bias correction was applied.

3.4 GCM data

The CGCM3 and ECHAM5 data are used in this paper. They both include the IPCC 20-th Century experiment (20c3m) for years 1850-2000. We chose 1971-2000 as our baseline because more observations are available to be compared during these decades. Both GCMs

provide enough required variables such as geopotential height, specific humidity, temperature, wind fields, surface pressure, mean sea level pressure, and sea surface temperature for downscaling. CGCM3 has two different horizontal resolutions; one of them is T47 horizontal resolution with 3.75x3.71 degrees longitude/latitude, providing 6-hour interval data with 31 sigma levels. The sigma level data are further converted to our required pressure level data for data pre-processing. ECHAM5 model data provide T63 horizontal resolution about 1.8750x1.86 degrees, also providing 6-hour interval data with 17 pressure levels. The SRES (Special Report Emissions Scenarios) A2 modeling results have the highest increased air temperature in the end of 21st century are considered in this paper.

4. Discussion of Results

4.1 Comparison between Rainfall Intensity of Rain Gauge and MM5 Simulations

We compared the MM5 simulated IDF curves with observations at the grid scale. As rain gauge data are point measurement and on the other hand MM5 simulated data are areal average (3km by 3km), therefore it is unreasonable to compare each rain gauge (RG) quantile (observation) with corresponding grid quantile (MM5 simulation) where the RG is located. Therefore, we did not attempt to do the direct comparison between RG and corresponding MM5 grid, instead we compared quantiles of the upper bound (maximum) and lower bound (minimum) from 13 rain gauges and 194 MM5 grids which belong to Edmonton.

Table 1. Upper bound of observed (1984-2010) rain gauge quantiles (mm/hr) for different return periods.

Duration (hr)	Return period (year)					
	2	5	10	25	50	100
0.25	37.95	55.23	67.40	83.68	96.44	109.72
0.5	24.01	35.89	45.06	58.37	69.66	82.22
1	14.85	22.27	28.02	36.40	43.54	51.51
2	9.38	13.93	17.27	21.92	25.70	29.75
6	4.46	6.30	7.50	9.00	10.10	11.19
12	2.73	3.85	4.62	5.64	6.43	7.24
24	1.67	2.45	3.02	3.80	4.43	5.09

The comparison between the upper bound and lower bound values of the observed and simulated rainfall intensity is shown in Figure 2. The results indicate toward gradually more intense heavy rainfalls in future climate. Table 1, 2 and 3 show the upper bound (maximum) values of the observed periods (1984-2010), the 2050s (2041-2070) and the 2080s (2071-2100). The relative change (% of change) in the 2050s and the 2080s with respect to the observed quantiles are shown in parentheses. In the 2050s, the maximum relative change in intensity is about 33% and 42% for the CGCM3 and ECHAM5 runs, respectively. On the other hand, in the 2080s, the maximum relative change was about 42% and 46% for the CGCM3 and ECHAM5 runs, respectively. In most of the cases, the relative increases are noticeably higher for the shorter duration (less than 6 hour) rainfall than the longer duration (6 hour or more) rainfall, especially in the 2080s which indicates toward more intensive convective rainfall in the 2080s. In the 2050s, changes were higher for the shorter return period (≤ 10 years) than for the longer return period (>10 years).

Table 2. Upper bounds of corrected MM5 simulated quantiles (mm/hr) of 2041-2070 for different return periods. The change percentages (%) with respect to observed quantiles are given in parentheses.

Duration	CGCM3/Return period (year)					
(hr)	2	5	10	25	50	100
0.25	45.33(19.42)	63.27(14.56)	75.63(12.20)	91.84(9.74)	104.33(8.17)	117.15(6.77)
0.5	30.13(25.49)	44.43(23.79)	55.39(22.92)	71.19(21.97)	84.51(21.32)	99.24(20.70)
1	19.33(30.24)	29.14(30.87)	36.80(31.34)	48.03(31.95)	57.65(32.41)	68.44(32.86)
2	11.78(25.56)	17.44(25.18)	21.68(25.50)	27.68(26.27)	32.64(27.02)	38.04(27.87)
6	4.93(10.53)	6.56(4.08)	7.60(1.28)	8.88(-1.39)	9.80(-2.97)	10.71(-4.29)
12	3.09(12.90)	4.03(4.70)	4.63(0.11)	5.36(-4.99)	5.89(-8.36)	6.42(-11.42)
24	1.93(15.98)	2.68(9.38)	3.15(4.50)	3.74(-1.63)	4.16(-6.01)	4.57(-10.18)
Duration	ECHAM5/Return period (year)					
(hr)	2	5	10	25	50	100
0.25	49.03(29.19)	66.04(19.57)	76.24(13.11)	88.21(5.41)	96.56(0.12)	104.45(-4.8)
0.5	31.10(29.56)	44.12(22.92)	52.99(17.60)	64.55(10.59)	73.41(5.40)	82.49(0.33)
1	19.19(29.26)	27.42(23.17)	33.35(19.02)	41.45(13.87)	47.96(10.16)	54.90(6.59)
2	11.32(20.65)	15.95(14.51)	19.26(11.50)	23.75(8.38)	27.34(6.40)	31.13(4.64)
6	5.14(15.16)	7.10(12.73)	8.46(12.75)	10.22(13.49)	11.55(14.28)	12.88(15.13)
12	3.14(15.01)	4.58(18.99)	5.70(23.34)	7.33(30.02)	8.72(35.63)	10.26(41.64)
24	1.88(12.98)	2.71(10.60)	3.31(9.75)	4.14(9.10)	4.82(8.82)	5.53(8.66)

Table 3. Upper bounds of corrected MM5 simulated quantiles (mm/hr) of 2071-2100 for different return periods. The change percentages (%) with respect to observed quantiles are given in parentheses.

Duration	CGCM3/Return period (year)					
(hr)	2	5	10	25	50	100
0.25	51.65(36.09)	70.77(28.14)	82.91(23.02)	97.82(16.89)	108.61(12.61)	119.14(8.59)
0.5	33.54(39.67)	48.99(36.49)	60.24(33.68)	75.70(29.70)	88.14(26.54)	101.37(23.30)
1	20.51(38.12)	30.83(38.46)	38.98(39.12)	51.04(40.22)	61.46(41.16)	73.24(42.19)
2	12.66(34.90)	18.91(35.73)	23.65(36.91)	30.43(38.82)	36.10(40.47)	42.32(42.26)
6	5.38(20.65)	7.39(17.24)	8.67(15.57)	10.25(13.85)	11.39(12.76)	12.51(11.81)
12	3.24(18.58)	4.38(13.88)	5.14(11.14)	6.10(8.03)	6.82(5.96)	7.54(4.06)
24	1.97(18.43)	2.80(14.56)	3.38(12.00)	4.14(8.90)	4.72(6.69)	5.33(4.58)
Duration	ECHAM5/Return period (year)					
(hr)	2	5	10	25	50	100
0.25	55.29(45.70)	76.91(39.26)	91.16(35.25)	109.28(30.58)	122.87(27.40)	136.55(24.46)
0.5	34.79(44.90)	51.43(43.28)	63.96(41.94)	81.79(40.15)	96.68(38.80)	113.02(37.47)
1	20.84(40.38)	30.92(38.83)	38.59(37.76)	49.68(36.46)	59.03(35.58)	69.42(34.76)
2	11.63(23.97)	16.82(20.75)	20.55(18.97)	25.65(17.02)	29.744(15.75)	34.10(14.62)
6	5.14(15.20)	7.099(12.70)	8.41(12.12)	10.073(11.90)	11.31(11.93)	12.53(12.04)
12	3.08(12.94)	4.416(14.75)	5.39(16.77)	6.763(19.85)	7.87(22.38)	9.05(25.06)
24	1.87(12.21)	2.64(7.91)	3.184(5.50)	3.90(2.75)	4.46(0.86)	5.045(-.90)

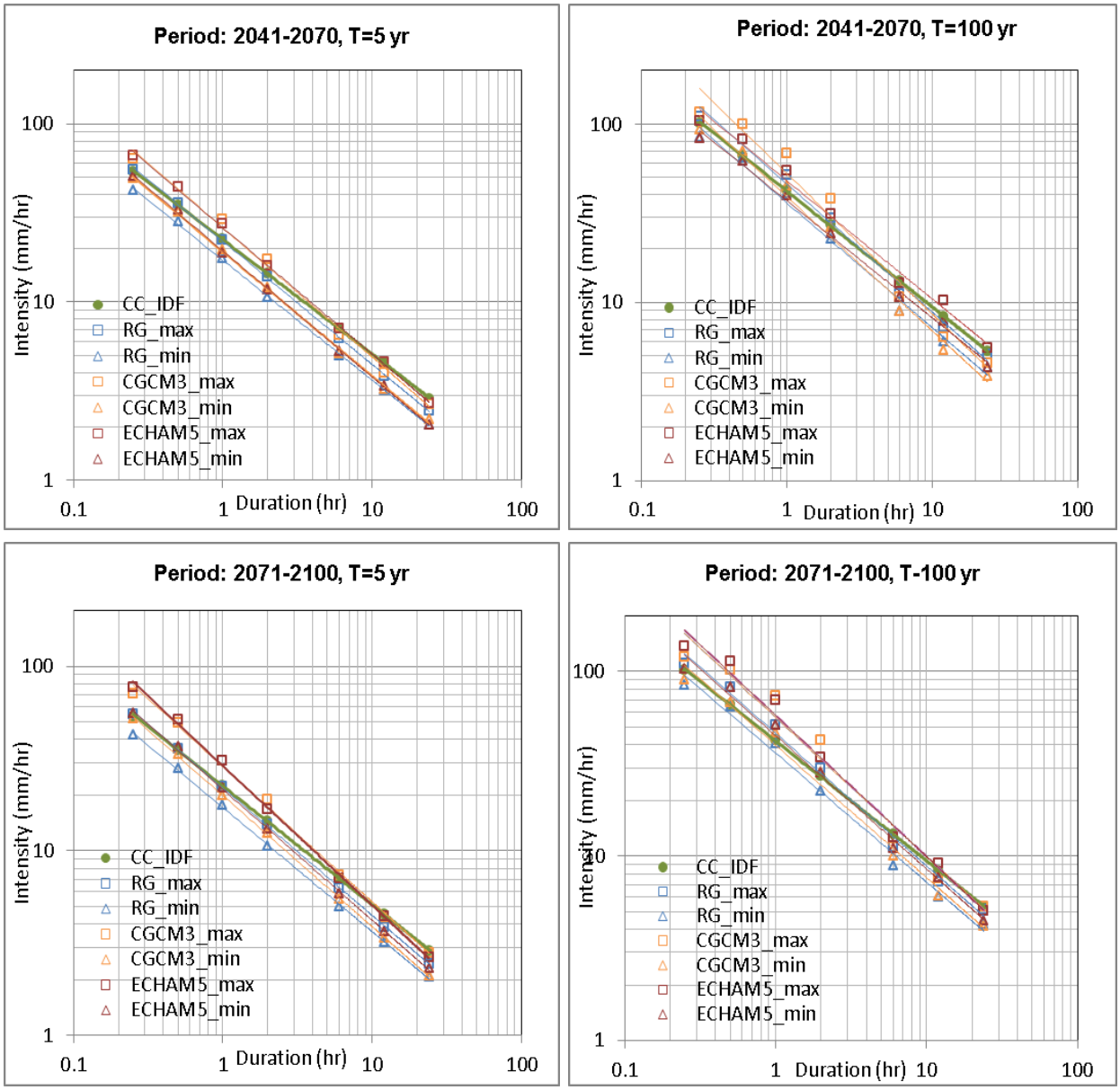

Figure 2. Comparison of current city IDF curve (CC_IDF), observed IDF curves based on rain gauge data of 1984-2010 (RG) and corrected MM5 simulated IDF curves of 2041-2070 (upper panel) and 2071- 2100 (lower panel).

In general, the projected IDF curves from the CGCM3 and ECHAM5 runs show similar trend. However, for the longer durations (six hours or more), ECHAM5 runs show similar or slightly higher intensity than the CGCM3 runs. On the other hand, for the shorter duration, ECHAM5 projected intensity is similar to CGCM3 projected intensity for the shorter return period (e.g., 5 year return period) but lower than the CGCM3 projected intensities for the longer return period (e.g., 100 year return period) in most of the cases.

The comparison between current city IDF curves and projected IDF curves is also shown in Figure 2. Comparison with the 2050s and 2080s shows that the current city IDF curve (CC_IDF) is following the lower bound of the projected IDF curves for durations less than 2 hours. On the other hand the CC_IDF lies around median (not shown) or slightly below the upper bound for

duration 2 hours or more for both 5 and 100 years return period. Overall, we conclude that CC_IDF is smaller than the projected upper bound for all durations, except 24-hour duration. In other words, we may suffer much intensive storm events for storm durations below 24 hours in a given return period. For the 24-hour duration, the projected IDF curves are about similar to CC_IDF curves.

4.2 Future projection of temperature and moisture

We have found that the rainfall intensity has been increased in both two runs under SRES A2. We further attempt to find out how other climate variables change. We found that the air temperature of D1 increase about 2 and 3ºC in central Alberta for 2050s and 2080s, respectively (not shown). The time series of D3 and its linear trend are further discussed.

The evaluated area is located in D3 and the data within about 30km length to the boundary has been discarded to avoid the boundary effect. The simulated spatial average 2-m air temperature time series from D3 for MJJA (May to August) is illustrated in Figure 3. The time series of simulated temperature between 2041 and 2100 are subtracted from their average between 1971 and 2000 to clearly show increasing (positive) or decreasing (negative) values in the future projection. Both CGCM3 and ECHAM5 runs have an increasing rate with 0.038 ºC per year and 0.054 ºC per year, respectively. The air temperature will increase about 3.5-4.0 ºC in the end of the century.

On the other hand, the precipitable water is also investigated. As expected, the simulated precipitable water increases for both runs as shown in Figure 4. It is not surprising because the higher the temperature, the more moisture can be held in the air. The increasing rate of simulated precipitable water of ECHAM5 run (0.096 mm/ year) is higher than that of CGCM3 run (0.056 mm/ year), which is consistent with the increasing rate of simulated air temperature for both runs.

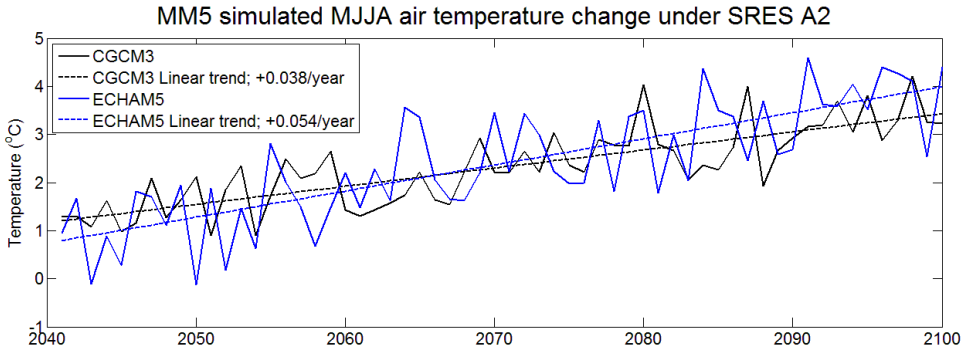

Figure 3. The time series of simulated MJJA (May to August) air temperature change for CGCM3 and ECHAM5 driven data in domain 3 under SRES A2.

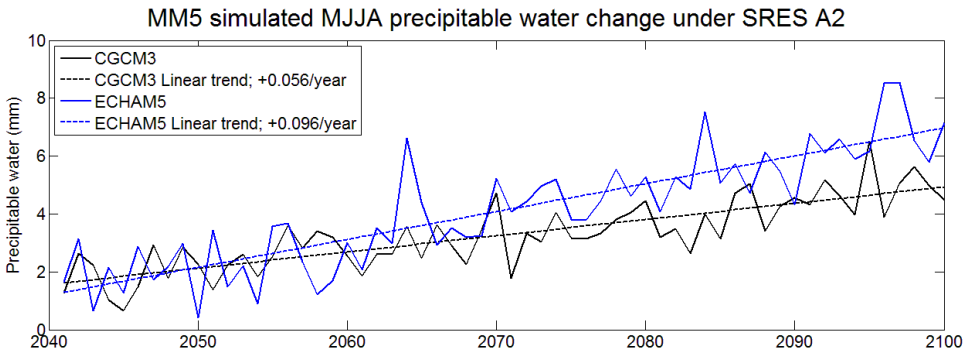

Figure 4. The time series of simulated MJJA (May to August) precipitable water for CGCM3 and ECHAM5 driven data in domain 3 under SRES A2.

Table 4. Average (AVG) and standard deviation (STD) of simulated surface temperature (ºC) and precipitable water (mm) among various periods under SRES A2

GCMs	Air temperature	1971-2000	2041-2070	2071-2100	Precipitable water	1971-2000	2041-2070	2071-2100
CGCM3	AVG	12.6	14.3	15.5	AVG	14.1	16.6	18.2
	STD	5.2	5.2	5.3	STD	4.3	5.1	5.8
ECHAM5	AVG	13.1	14.7	16.2	AVG	15.8	18.5	21.4
	STD	5.1	5.0	5.0	STD	5.0	5.9	6.8

Alternatively, the simulated 6-hr air temperature and precipitable water are presented in probability distribution (PD) as shown in Figure 5 and 6. The PD of the projected air temperature is shifted toward to the higher range without changing much of the shape of PD. The increased probability of higher precipitable water is shown in the two future runs. The detail of the average and standard deviation of simulated surface temperature and percipitable water is listed in Table 4. Overall, the average simulated air temperature increases in the 2050s and 2080s and the simulated air temperature standard deviation keep similar for both control and future runs. In addition, the average and standard deviation of simulated precipitable water increases in the 2050s and 2080s. The statistics give the idea that the moisture is expected to vary more and have more chance of higher moisture content in the future under SRES A2. This explains our simulations of the higher simulated rainfall intensity for both driven GCMs data in the 2050s and 2080s under SRES A2.

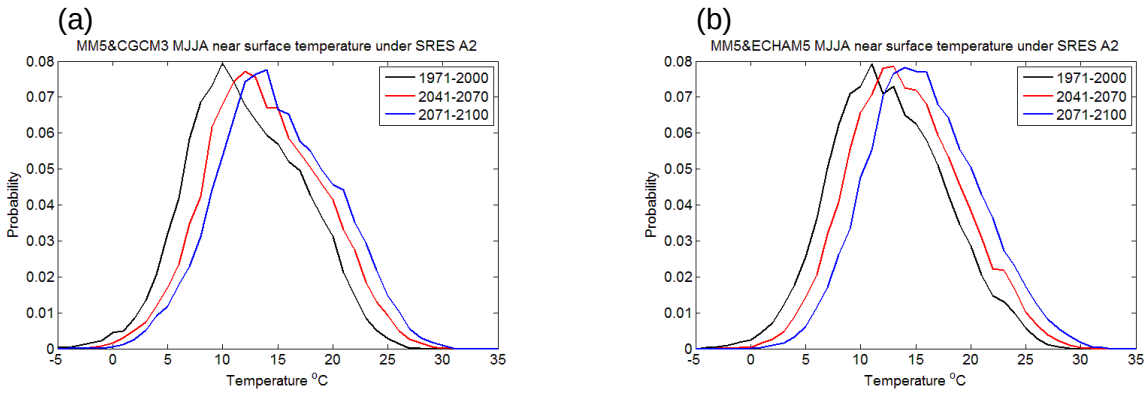

Figure 5. The probability distribution of the air temperature for (a) CGCM3 and (b) ECHAM5 driven data in domain 3 under SRES A2.

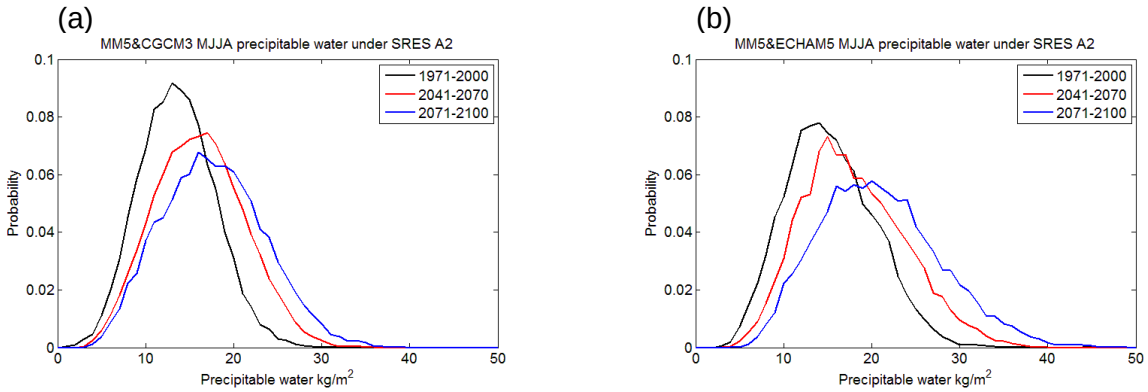

Figure 6. The probability distribution of the precipitable water for (a) CGCM3 and (b) ECHAM5 driven data in domain 3 under SRES A2.

5. Summary and Conclusions

We have used a regional climate model, MM5, to simulate baseline (1971-2000) and future (2041-2100) regional climate forced by CGCM3 and ECHAM5 data with SRES A2 in central Alberta. The simulated precipitation is used to develop the grid-based IDF curves. Due to modeling bias, the simulated precipitation is adjusted by a quantile-based bias correction before deriving the IDF curves. Next, the projected IDF curves are compared to the currently used IDF curves. Temperature and moisture trends are also investigated in this paper.

We found the projected IDF curves shift toward to higher intensity in all return periods, which is consistent with the increased temperature and moisture found in CGCM3 and ECHAM5 downscaling runs. The short durations' (d < 6 hours) rainfall intensities (upper bound) are expected to increase up to 42 and 46% for the 2050s (2041-2070) and 2080s (2071-2100), respectively. The current city IDF curves are generally below the upper bound of IDF curves for the 2050s and 2080s between 15-minute and 12-hour durations. Therefore, the current standards are likely under-designed if we keep the current IDF curves for hydrological infrastructure designing.

The increased rainfall intensity is stemmed from the increased temperature which provides the extended amount of moisture in this area, leading more moisture in different levels of atmosphere. Overall, the simulated average precipitable water of ECHAM5 (CGCM3) runs have increased from 15.8 (14.1) mm of control run to 18.5 (16.6) and 21.4 (18.1) mm for 2050s and 2080s, respectively. We also found that the simulated air temperature and precipitable water for 2041-2100 have gradually upward trend. The probability distribution of simulated air temperature and precipitable water also reveal their increased trends.

Although the future projection of rainfall intensity shows increased rainfall intensity under SRES A2 condition of CGCM3 and ECHAM5, we cannot just conclude that the IDF curves will shift toward with this range of intensities because dynamical downscaling of several GCMs' projections for the same SRES climate scenario lead to different storm simulations. Therefore, future work will include more GCMs' data as our forcing conditions in order to consider the uncertainty stemmed from GCMs.

6. References

[1] Allan R.P. and Soden B.J., "Atmospheric warming and the amplification of precipitation extremes", *Science*, Vol. 321, 2008, pp.1481-1484.

[2] Dore M.H.I, "Climate change and changes in global precipitation patterns: What do we know?" *Environment International*, Vol. 31, 2005, pp.1167-1181.

[3] Erfani A., Methot A., Goodson R., Belair S., Yeh K., Cote J., and Moffet R., "Synoptic and Mesoscale Study of a Severe Convective Outbreak with the Nonhydrostatic Global Environmental Multiscale (GEM) model", *Meteorology and Atmospheric Physics*, 2003, Vol. 82, pp.31-53.

[4] Fowler H. J., Ekstrom M., Kilsby C. G., and Jones P. D., "New estimates of future changes in extreme rainfall across the UK using regional climate model integrations. 1: Assessment of control climate", *Journal o Hydrology*, Vol. 300, 2005, pp. 212–233.

[5] Hamlet A. F. and Lettenmaier D. P., "Effects of 20th century warming and climate variability on flood risks in the western U.S.", *Water Resources Res*earch, 2007, Vol. 43, Iss. 6, pp. W06427.

[6] Hosking J. R. M. and Wallis J. R., "Regional Frequency Analysis: An Approach Based on L-Moments", Cambridge University Press, 2007.

[7] Kain J.S., "The Kain–Fritsch Convective Parameterization: An Update", *Journal of Applied Meteorology*, Vol. 43, 2004, pp.170-181.

[8] Kuo C.C., Gan T. Y., and Chan S., "Regional Intensity-Duration-Frequency Curves Derived from Ensemble Empirical Mode Decomposition and Scaling Property", *Journal of Hydrologic Engineering*, Vol. 18, 2013, pp. 66-74.

[9] Lafon T., Dadson S., Buys G. and Prudhomme C., "Bias correction of daily precipitation simulated by a regional climate model: a comparison of methods", *International Journal of Climatology*, 2012, DOI: 10.1002/joc.3518.

[10] Laprise R., Caya D., Frigon A. and Paquin D., "Current and perturbed climate as simulated by the second-generation Canadian Regional Climate Model (CRCM-II) over northwestern North America", *Climate Dynamics*, Vol. 21, 2003, pp. 405-421.

[11] Lenderink G. and Van Meijgaard E., "Increase in hourly precipitation extremes beyond expectations from temperature changes", *Nature Geoscience*, Vol. 1, 2008, pp. 511-514.

[12] Mailhot A., Duchesne S., Caya D., and Talbot G., "Assessment of future change in intensity–duration–frequency (IDF) curves for Southern Quebec using the Canadian Regional Climate Model (CRCM)", *Journal of Hydrology*, Vol. 347, 2007, pp. 197–210.

[13] Mailhot A., Beauregard I., Talbot G., Caya D., and Biner S., "Future changes in intense precipitation over Canada assessed from multi-model NARCCAP ensemble simulations", *International Journal of Climatology*, Vol. 32, 2012, pp. 1151-1163.

[14] Milly P.C.D., Dunne K.A., Vecchia A.V., "Global pattern of trends in streamflow and water availability in a changing climate", *Nature*, Vol. 438, 2005, pp. 347-350.

[15] Mladjic B., Sushama L., Khaliq M.N., Laprise R., Caya D., and Roy R., "Canadian RCM projected changes to extreme precipitation characteristics over Canada", *J. Climate*, Vol. 24, 2011, pp. 2565-2584.

[16] Mlawer E.J., Taubman S.J., Brown P.D., Iacono M.J., and Clough S.A., "Radiative Transfer for Inhomogeneous Atmospheres: RRTM, a Validated Correlated-k Model for the Longwave", *Journal of Geophysical Research*, Vol. 102, 1997, pp. 16663-16682.

[17] Reisner J., Rasmussen R.M., and Bruintjes R.T., "Explicit Forecasting of Supercooled Liquid Water in Winter Storms using the MM5 Mesoscale Model", *Quarterly Journal of the Royal Meteorological Society*, Vol. 124 B, 1997, pp. 1071-1107.

[18] Schmidli J., Frei, C., and Vidale P.L., "Downscaling from GCM precipitation: a benchmark for dynamical and statistical downscaling methods", *International Journal of Climatology*, Vol. 26, 2006, pp. 679–689.
[19] Shen S.S.P., Yin H., Cannon K., Howard A., and Chetner S., "Temporal and spatial changes of the agroclimate in Alberta, Canada, from 1901 to 2002", *Journal of Applied Meteorology*, Vol. 44, 2005, pp. 1090-1105.
[20] Shepherd A. and McGinn S.M., "Assessment of climate change on the Canadian Prairies from downscaled GCM data", *Atmosphere-Ocean*, Vol. 41, Iss. 4, 2003, pp. 301-316.
[21] Sun Y., Solomon S., Dai A., and Portmann R.W., "How often will it rain?", *Journal of Climate*, Vol. 20, 2007, pp. 4801-4818.
[22] Wang B., Bao Q., Hoskins B., Wu G., and Liu Y., "Tibetian Plateau warming and precipitation changes in East Asia", *Geophysical Research Letter*, Vol. 35, Iss. 14, 2008, pp. L14702.
[23] Wood A.W., Leung L. R., Sridhar V., and Lettenmaier D. P., "Hydrologic implications of dynamical and statistical approaches to downscaling climate model outputs", *Climatic Change*, Vol. 62, 2004, pp. 189–216.

7. Acknowledgements

We are grateful to Compute Canada's WestGrid support staff for their assistance with technical issues. This research was supported by the City of Edmonton and Natural Sciences and Engineering Research Council.

8. Biography

Dr. Chun-Chao Kuo and Dr. Nasreen Jahan are currently Postdoctoral Researchers at University of Alberta's water resources engineering. Mesgana Gizaw is currently a PhD student in Dr. Thian Yew Gan's group. Dr. Gan is a professor at University of Alberta since 1993 and a fellow of the American Society of Civil Engineers (ASCE). Steven Chan is a Senior Assessment Engineer in urban sewer system assessment.